New Insight into Fluorescent Polymeric Carbon Dots for Solid-State Laser Device

Barun Kumar Barman,[1*] David Hernández-Pinilla,[1*] Ovidiu Cretu,[3] Riichiro Ohta,[4*] Keiko Okano,[1] Toshifumi Shiroya,[4] Jun Sasai,[4] Koji Kimoto,[3] and Tadaaki Nagao [1, 2*]

[1]International Center for Materials Nanoarchitectonics (WPI-MANA), National Institute for Materials Science (NIMS), Tsukuba, Ibaraki 305-0044, Japan

[2]Department of Condensed Matter Physics Graduate School of Science, Hokkaido University, Kita-10 Nishi-8 Kita-ku, Sapporo 060-0810, Japan

[3]Electron Microscopy Group, National Institute for Materials Science (NIMS), Tsukuba, Ibaraki 305-0044, Japan

[4]L'Oréal Research and Innovation, KSP R&D, 3-2-1 Sakado, Takatsu-ku, Kawasaki, Kanagawa 213-0012, Japan

Email: BARMAN.Kumarbarun@nims.go.jp

mayphys87@gmail.com

riichiro.ohta@loreal.com

NAGAO.Tadaaki@nims.go.jp

Abstract: Polymeric carbon dots (PCDs) are an astonishing class of fluorescent materials with distinctive structures, properties, and applications. However, internal structures of PCDs are still unclear and are the subject of considerable debate, due to their complexity. Herein, a new type of pure blue light-emitting PCDs was synthesized hydrothermally from ε-poly-L-lysine and citric acid. PCDs were observed using scanning transmission electron microscopy coupled with electron energy loss spectroscopy (STEM-EELS) on an atomically thin graphene surface to determine the internal structure and compositional gradients combined with other spectroscopic analyses. These methods revealed that PCDs have a spongy, porous structure with uniform element distribution, reflecting organic polymeric frameworks that embrace fluorescent aromatic moieties, devoid of graphitic, inorganic carbon. The polymeric framework acts as a transparent matrix and effectively resists self-quenching of photoluminescence (PL) in solid-state. Exploiting their excellent fluorescence properties, PCDs embedded in a planar microcavity composed of two distributed Bragg reflectors (DBR), which was demonstrated as a single longitudinal solid-state blue laser. The results will facilitate detailed understanding of internal structures of PCDs and their efficient, solid-state emission toward development of rare-earth-free lighting devices.

Keywords: Polymeric carbon dots, internal structure, scanning transmission electron microscopy, solid-state emission, photonic cavity, laser device.

Introduction

Carbon dots (CDs), a new class of carbon-based nanostructures, have generated great interest from the research community due to their unique optical properties, photo-stability, and low cost.[1-9] Since CDs are mostly composed of C, O, and H, and are completely metal-free, many research groups anticipate that CDs will ultimately replace RE-doped phosphors, metal chalcogenide-based quantum dots, and perovskite quantum dots. Another advantage of CDs compared to other quantum dots is that they can easily be synthesized bottom-up from various organic molecules via chemical methods.[10-15] Optical properties of CDs depend strongly on their chemical composition, chemical bonding states, structure, surface functionalization, dopants, etc. Structures of CDs include crystalline, amorphous, molecular assembles, and polymeric structures,[16-25] some of which have not been proven to contain graphitic, inorganic carbon. CD photoluminescence originates mainly from the surface state, subdomain state, molecular state, and crosslink-enhanced emission (CEE) effect. The molecular state and CEE effect predominantly dictate their optical properties.[20, 21, 26-29] CDs derived from citric acid (CA) and amine precursors, e.g., 1,2-ethylenediamine, ammonia, urea, exhibit strong blue fluorescence (FL) with high photoluminescence quantum yields (PLQY) due to presence of heteroaromatic moieties (1,2,3,5-tetrahydro-5-oxo-imidazo[1,2-a]pyridine-7-carboxylic acid (IPCA), citrazinic acid (CZA), 4-hydroxy-1H-pyrrolo[3,4-c]pyridine-1,3,6 (2H,5H)-trione (HPPT)), which are produced via condensation of carboxy groups in CA and amine groups and which contribute much of the blue emission,[30, 31] while supramolecular ionic materials exhibiting fluorescence can be reportedly produced from CA and 1-(2-aminoethyl) piperazine (AEPZ) via non-covalent interaction just by drying out the solvent, [32] implying that the origins of their optical properties are diverse and remain vague for some cases. Recently, various research groups have developed a new kind of CD, termed carbonized polymer dots (CPDs), consisting of both polymer and carbon hybrid structure. These dots not only possess the unique optical properties of conventional CDs, but also inherit the softness of polymeric materials. They contain a large amount of N and O, aqueous solubility, and high PLQY, and have been synthesized via crosslinking and polymerization of small molecules and polymers.[27, 33-48] Some reports insist that these dots are composed of tiny carbon clusters surrounded by highly dehydrated cross-linking and close-knit polymeric framework; however, these structures are still unclear and the subject of considerable debate due to their complexity and limitations of microscopic observation. For observation via transmission electron microscopy, due to low contrast between carbonized polymer dots and carbon-coated copper grids, brightfield images of carbonized polymer dots are seldom sufficiently distinct. There are also concerns about graphitic artifacts in the observed images, which reportedly stem from graphitic contaminants in carbon-coated grids[49] and structural ordering due to electron irradiation during observation.[50] It is essential to resolve the aforementioned points, as well as to determine the internal structures of the dots via both spectroscopic and microscopic methods. Accordingly, electron energy loss spectroscopy (EELS) in a scanning

transmission electron microscope (STEM) mode operated at low voltage can enable spectroscopic mapping of structures with a tightly focused electron beam that scan across the nano specimen. Interactions between primary electrons in the STEM probe and bound electrons in a single dot are measured directly, which provides rich chemical information down to atomic scale.

In the present study, a new type of pure blue light-emitting polymeric carbon dots (PCDs) was synthesized by hydrothermally reacting CA and ε-poly-L-lysine (PLys) of uniform hydrodynamic size in the range 4-10 nm (avg. 5.5 nm) with absolute PLQY as high as 49 %. These PCDs were observed using STEM-EELS to determine the structure, compositional gradients, and elemental distribution. STEM-EELS observations combined with results of nuclear magnetic resonance spectroscopy, X-ray photoelectron spectroscopy, vibrational analyses, dynamic light scattering, and total carbon analysis revealed that these PCDs do not contain graphitic, inorganic carbon, but possess an amorphous polymeric structure composed of tiny clusters with uniform element distribution, having an organic polymeric framework embracing fluorescent, aromatic moieties. Interestingly, because the fluorescent aromatic moieties are enclosed in a polymeric framework, self-quenching of PLs was inhibited in solid form. Spectroscopic analysis revealed that PL centers formed by pyridinic moieties embraced in polymeric frameworks are the indispensable, basic building blocks of blue luminophores, responsible for the high luminescence of PCDs. Finally, using a planar microcavity with only one resonant mode, coupled with emission of PCDs, a single, longitudinal, solid-state, blue laser device has been constructed. The results in this study will aid detailed understanding of PCDs and will promote efficient, solid-state emission toward development of completely rare-earth-free lighting devices.

Experimental Section

PCD synthesis

PLys (25 w/v % aqueous solution, ~36 mer, molecular weight 4600 g mol^{-1}) was purchased from JNC Corporation (Tokyo, Japan). CA monohydrate was purchased from FUJIFILM Wako Pure Chemical Corporation. All chemicals were used without further purification. CA monohydrate (0.48 M, ~2.5 g) and 4 wt.% of PLys (~1 g) solution were mixed in 25 mL Milli-Q water via sonication for ~3 min. The transparent mixture solution was then transferred to a 50-mL polytetrafluoroethylene vessel and placed in a stainless-steel autoclave crucible for hydrothermal reaction. The solution was heated at 180 °C for 4 h for synthesis of PCDs and then cooled to room temperature to produce a yellowish supernatant dispersion along with agglomerated sticky material. The dispersion was centrifuged at 8000 rpm for 5 min and passed through a 0.2-μm syringe filter to remove aggregates and large particles. Then the solvent was evaporated by heating on a hot plate followed by heating in a vacuum furnace at 110 °C to remove excess water, resulting in a yellowish powder. After centrifugation and filtering, PCDs were utilized as synthesized for further characterization and for optical gain experiments.

Material characterization

The crystallinity of as-prepared samples was characterized using X-ray diffraction (XRD; RINT-Ultima III, Rigaku Corporation) equipped with Cu Kα radiation (λ = 1.5406 Å). The composition and chemical bonding states of PCDs were characterized using CHNO elemental analysis, X-ray photoelectron spectroscopy (XPS), nuclear magnetic resonance spectroscopy (NMR), and attenuated total reflection-Fourier transform infrared spectroscopy (ATR-FTIR). XPS was performed using a PHI Quantera SXM (ULVAC-PHI, Inc.) with Al Kα as an X-ray source. ATR-FTIR employed a Nicolet iS50 FTIR instrument (Thermo Fisher Scientific Inc.) under vacuum conditions to minimize the influence of atmospheric gases, including humidity. Each spectrum was collected with 50 accumulated scans. The measurement of Raman spectra was performed in an Alpha 300S microscope (WITec GmbH) by using a 785 nm laser source (Toptica photonics, Inc.) with 30 accumulated scans for each spectrum. ^{1}H and ^{13}C NMR were performed on PCDs, PLys, and CA using dimethyl sulfoxide-D6, D_2O, and MeOD as solvents. The amount of organic carbon (OC) and graphitic inorganic carbon (hereinafter, referred to as elemental carbon (EC) as described in the evaluation guide previously issue) [42] in PCDs were analyzed using a total carbon analysis (Lab OC-EC Aerosol Analyzer, Sunset Laboratory Inc.) coupled with correction utilizing optical reflectance. Specimens were prepared for analysis by dropping a dispersion of PCDs on a quartz filter (2500QAT-UP, TOKYO DYLEC CORP.), and then evaporating the solvent. Amounts of OC and EC were estimated from the amount of CO_2 produced by heating the specimen in a He atmosphere at 250°C, 450°C, 500°C, and 550°C and in He/O_2 (98%/2%) atmosphere at 550°C, 700°C, 800°C, 870°C, 920°C, and 950 °C, respectively, as described in the evaluation guide.[51] The amount of CO_2 was quantified by detecting CH_4 produced after reduction of CO_2 using a flame ionization detector. An aqueous solution of commercial graphene oxide (highly concentrated graphene oxide dispersion in water, concentration: 5g L^{-1}, composition: carbon (≥ 46%), oxygen (≤ 46%), thickness: 1 atomic layer - at least 60%., color: brown, Graphene Supermarket®, Graphene Laboratories Inc.) was used for comparison. Amounts and concentrations of each sample are summarized in Table 1.

Table 1. Amounts and concentrations of dispersions of graphene oxide and PCDs dropped onto a quartz filter for total carbon analysis

Sample	Concentration (μg mg^{-1})	Weight of the droplet (mg)	Weight of the solid component (μg)
Graphene oxide	2.75	8.69	23.9
PCDs	4.0	8.86	35.4

The hydrodynamic size of PCDs in the dispersion was estimated using dynamic light scattering (ELSZ-2000, Otsuka Electronics Co., Ltd.). CONTIN was used as the analytical method of the autocorrelation function. PCDs were also characterized via transmission electron microscopy (TEM) using a Titan (Thermo Fisher Scientific Inc.) electron microscope in scanning (STEM) mode, equipped with a Quantum EELS spectrometer (Gatan, Inc.). STEM-EELS analysis was conducted at relatively low voltage (80 kV) so as to minimize damage due to electron irradiation, which reportedly causes crystallization of amorphous carbon to form carbon onions over 100 kV.[60] The size of the probe was approximately 0.2 nm, and the probe current was set to ~50 pA. Images were acquired using an annular dark-field (ADF) detector. Samples were prepared by drop-casting diluted aqueous dispersions onto TEM grids covered with either amorphous carbon (with a thickness of ~ 6 nm) or several layers of graphene oxide (GO), which is sufficiently flat for observation of substances of nano-scale height. Some samples were heated at 150 °C for 5 min in a high vacuum (10^{-4} Pa) prior to observation. Topography of PCDs dispersed on Si substrates was observed under ambient conditions using an atomic force microscope (AFM; SPA-400, SPI-3800N, Seiko Instruments Inc.) with a Si probe (SI-DF40, Seiko Instruments Inc.; force constant = 48 N m^{-1}) in dynamic force mode (DFM). A V-570 UV−VIS−NIR spectrometer (JASCO Corporation) was used to collect absorbance spectra of both dispersions and films. Fluorescence spectra were collected using a FP8500 spectrometer (JASCO Corporation). Absolute PLQYs of PCDs dispersions and their films were measured under atmospheric conditions using a C9920-02G integrating sphere system (Hamamatsu Photonics K.K.). The laser experiment was performed using a 10x objective with a numerical aperture of 0,30. The pump beam (wavelength of 355 nm) focused by this objective has a spot radius of 0.77 μm.

Mirror fabrication and characterization

Distributed Bragg reflector (DBR) architectures were designed via optical simulations using the rigorous coupled-wave analysis (RCWA) numerical technique from RSoft software (Synopsys, Inc.). Optical constants of AlN and SiO_2 were experimentally obtained via spectroscopic ellipsometry of actual sputtered thin films in the Namiki Foundry at the Research Division for Material Nanoarchitectonics (MANA, NIMS), using a SE850DUV ellipsometer (SENTECH Instruments GmbH). Following the simulation results, mirrors consisting of 17 alternating AlN and SiO_2 layers with thicknesses of 48 nm and 72 nm were prepared on clean quartz substrates via 300 W RF sputtering (i-Miller CFS-4EP-LL, Shibaura Megatronics Corporation). AlN layers were deposited under a mixed 18 sccm Ar and 2 sccm N_2 atmosphere while SiO_2 layers were prepared under a pure 20 sccm Ar after evacuation to a $3.5x10^{-5}$ Pa base pressure. The optical response of sputtered DBR mirrors was measured using a V-570 UV-VIS-NIR spectrophotometer (JASCO Corporation). Cross-sectional images of the mirrors were observed using an S-4800 Scanning Electron Microscope (SEM; Hitachi High-Tech) at the Namiki Foundry at NIMS.

Results and Discussion

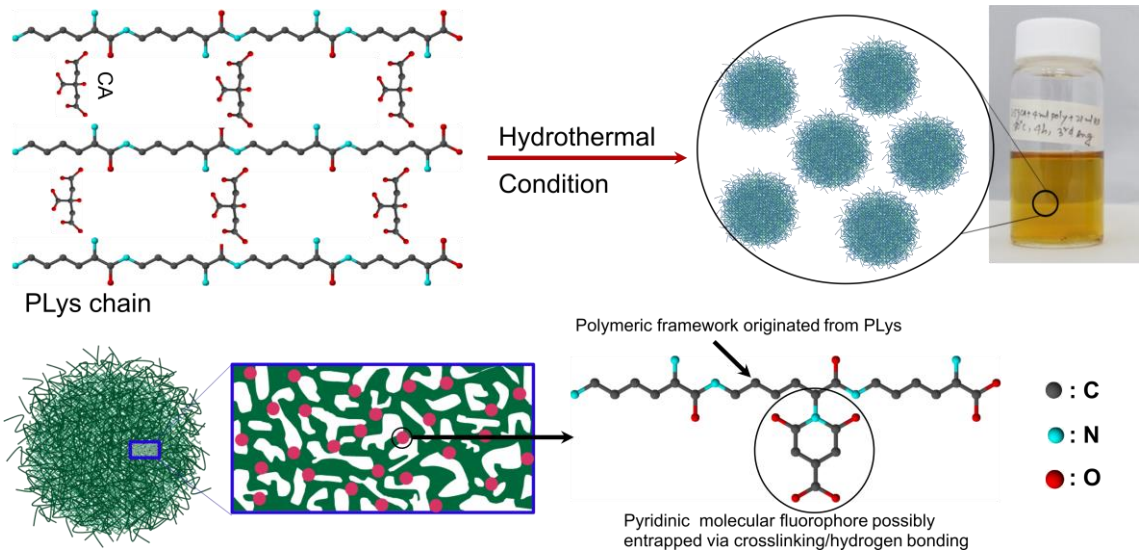

Figure 1. Schematic representation of PCD formation via a hydrothermal reaction between CA and PLys. Schematic representation of potential structure in PCDs with molecular fluorophores.

The yellowish dispersion (Figure 1) of PCDs was produced from CA and PLys via hydrothermal reaction at 180 ˚C for 4 h. The reason for using PLys as a coupling agent was to promote a nucleophilic reaction between the amine group of PLys and the carboxyl group of CA to potentially form amide bonds and small molecular fluorophore (Figure 1). The structure of as synthesized PCDs was characterized with various characterization methods. Figure 2a shows the XRD patterns of PLys and PCDs. PLys is a peptide polymer that can form α-helices, β-sheets, and random coil structures in solid states. For this reason, multiple XRD peaks at 2θ=~21 appear, corresponding to different conformations of peptide structure.[52] After the hydrothermal reaction, a broad peak at 2θ=~21 appeared and multiple peaks corresponding to PLys disappeared, indicating formation of a disordered, amorphous structure. Chemical functional groups in PCDs were further analyzed using ATR-FTIR (Figure 2 b). Broad, strong peaks appeared from 3500 to 2100 cm^{-1} in the PCD spectrum. Peaks at 3000-3500 cm^{-1} correspond to the stretching vibration of NH_3^+, -NH, and -OH bonds.[17, 30] Peaks at 2570 cm^{-1} correspond to the O-H stretching vibration in -COOH groups. Peaks at 3000 cm^{-1} correspond to C-H stretching vibrations.[53-55] These peaks are broader than those in the spectrum of PLys, implying that chemical bonding states, including these functional groups are more diverse in PCDs than those in PLys. The peaks of -COOH groups at 2570 cm^{-1}, as well as a very sharp peak at 1700 cm^{-1} corresponding to the C=O stretching vibration, did not appear in the spectrum of PLys but only in that of PCDs, indicating that unreacted -COOH groups of CA remain in the PCDs.

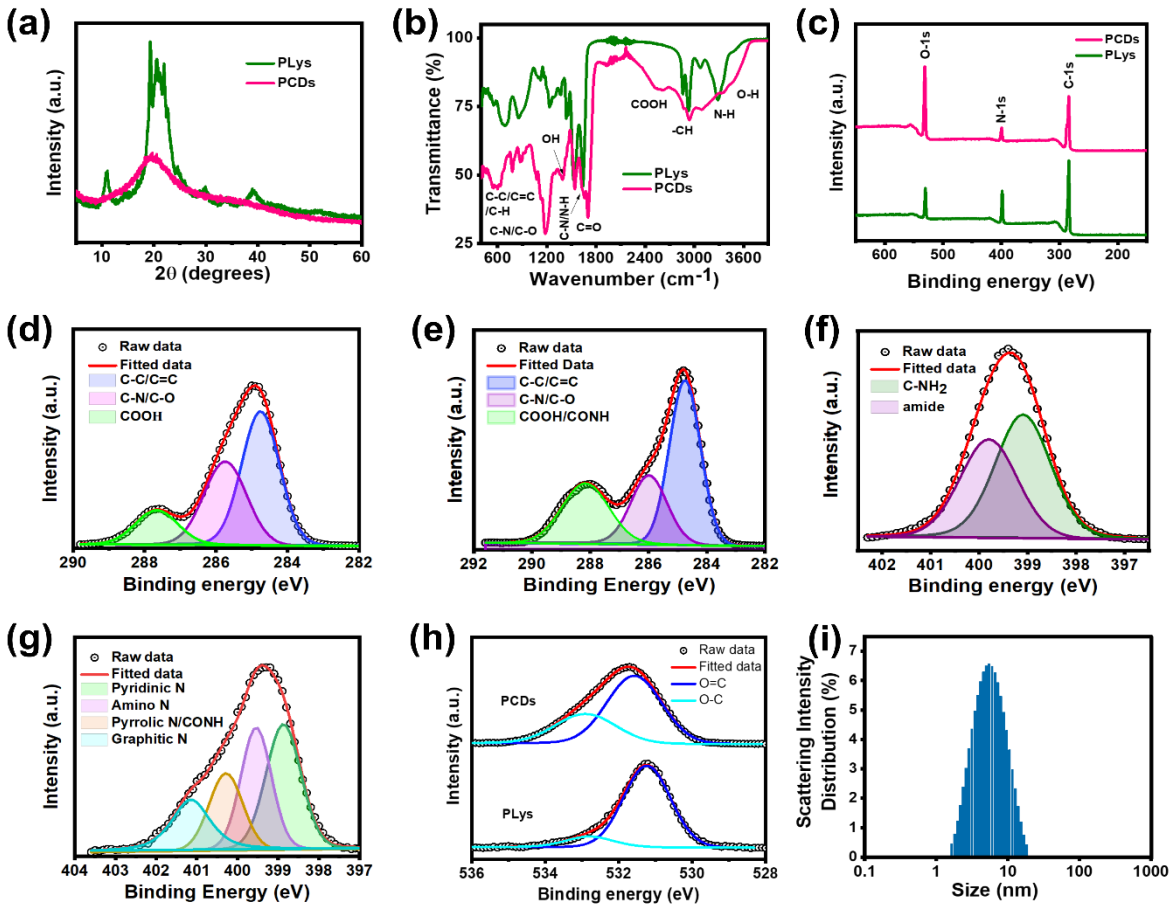

Figure 2. (a-c) XRD pattern, ATR-FTIR, and XPS survey spectra of PLys and PCDs. De-convoluted XPS spectra of (d,e) C-1s and (f,g) N-1s of PLys and PCDs. (h) Comparison of O-1s spectra of PLys and PCDs. (i) Scattering light distribution of PCDs dispersion obtained via DLS.

The intensity of a sharp peak that appeared at 1178 cm^{-1} in the spectrum of PCDs was higher than that of PLys. This peak may be assigned to the C-O stretching vibration mode in -COOH groups. Other peaks in the fingerprint region (<1500 cm^{-1}) in the spectrum appeared similar to those of PLys, while their positions were slightly different. Compositions of PLys and PCDs determined using CHNO analysis are summarized in Table S1. The H/C and N/C atomic ratios of PLys are 2.10 and 0.33, but decreased to 1.40 and 0.12, respectively, in PCDs, whereas the O/C ratio increased from 0.17 to 0.70 after the hydrothermal reaction. This resulted from the reaction of PLys with CA, which contains a lower proportion of N and H atoms and a higher proportion of O atoms than PLys. Table 2 shows the result of total carbon analysis of PCDs in comparison with that of commercial graphene oxide. All carbon was detected as OC and the amount of EC corresponding to graphitic inorganic carbon was less than the detection limit of the analytical method, indicating that PCDs are mainly composed of

materials with organic characteristics. The weight (18 μg) of total carbon was almost half of the weight (35.4 μg) of the solid component in the dispersion subjected to analysis. The residual weight of the solid component originates from H, N, and O atoms, according to CHNO elemental analysis (Table S1). The significant amount of elements other than C implies the presence of chemical functional groups responsible for the organic characteristics of PCDs. XPS survey spectra also revealed the presence of C, O, and N atoms in PCDs (Figure 2c). The atomic ratio in PCDs obtained via XPS survey was C:O:N (63.7/28.8/7.5), in which a large amount of oxygen was present in PCDs, similar to the atomic ratio of C:O:N (55.1/38.6/6.3) by excluding H atoms from the CHNO analytical result (Table S1). The larger amount of C atoms seen in XPS results relative to CHNO analysis may be attributed to surface contamination of PCDs because XPS is more surface-sensitive than CHNO analysis. Figures 2d and e display the deconvoluted C-1s peaks of PLys and PCDs. The peak at 284.8 eV can be attributed to sp^3 hybridized and sp^2 hybridized C atoms in carbon networks or those bound to H atoms. The peaks assigned to C atoms bound to N atoms and those bound to O atoms are located at 285.7 eV. The peak at 287.7 eV corresponds to C atoms in peptide bonds (Figure 2. d).[17, 55] After formation of PCDs, the high binding energy peak at 288.4 eV attributed to C atoms in carboxylate and amide groups is shifted by 0.7 eV to higher binding energy with respect to bare peptide bonds. Deconvoluted spectra also show an increase of COOH functional groups in PCDs compared to PLys and a decrease of C-N%. Figures 2f and g show deconvoluted N-1s spectra of PLys and PCDs, respectively. The spectrum of PLys comprises two major configurations corresponding to N atoms in amide and amine functional groups. The N-1s peak deconvoluted to multiple peaks attributed to pyridinic-N (398.8 eV), amine (399.6 eV), amide/pyrrolic N (400.3 eV), and graphitic N (401.3 eV) (Figure 2g).[56-58] Figure 2h shows a comparison of O-1s spectra of PLys and PCDs. Both spectra consist of two peaks at ~531 eV and at ~533 eV, which may be assigned to O atoms bound to C atoms with double bonds (O=C) and O atoms bound to C atoms with single bonds (O-C), respectively.[59] The O-1s spectrum of PLys mainly comprised the peak assigned to O=C, which is consistent with its molecular structure. The ratio (~34 %) of peak assigned to O-C in the spectrum PCDs was larger than that (~12 %) in the spectrum of PLys. This implies the presence of chemical structures similar to those of CZA and the remaining CA in the PCDs, which are further discussed below on the basis of NMR spectra. ^{1}H and ^{13}C NMR spectra of PCDs, PLys, and CA were collected to further reveal chemical bonding states. The ^{1}H NMR spectrum of PCDs is shown in Figure S1. When compared with the spectrum of the precursors, peaks (~2.5-2.6 ppm) positioned close to those of CA (Figure S2) were detected. Since intensities of these peaks are strong, structures assigned to them are likely present in relatively high concentrations. Peaks (1-2 ppm) of protons in hydrocarbons bonded to C atoms, and peaks (3-3.5 ppm) of protons in hydrocarbons bonded to N atoms in the spectrum of PCDs appeared close to those in the spectrum of PLys (Figure S3), indicating that the PLys framework remains in the

PCDs. The broadening of peaks at 1-2 ppm in the spectrum of PCDs is attributable to the disordering of the PLys crystalline structure, which was confirmed via XRD analysis (Figure 2a). The peaks at 4.0-4.5 ppm in the spectrum of PCDs can be potentially assigned to protons in methine groups neighboring amide bonds, which implies the formation of crosslinking between the PLys framework and fluorophores. The peak at ~13 ppm in the spectrum of PCDs disappeared after addition of D_2O, indicating that the peak is assigned to protons in a carboxylic acid (Figure S4). There are numerous small peaks at 5.7 ppm to 7.5 ppm corresponding to protons in pyridinic and aromatic structures in the spectrum of PCDs. The peak appearing at 5.7 ppm in the spectrum of PCDs located close to the calculated chemical shift for protons bound to aromatic carbon in one tautomer of de-protonated CZA (CZA1MA).[60] The peak appearing at 6.5 ppm in the spectrum of PCDs located close to the calculated chemical shift for protons bound to aromatic carbon and heteroatoms in another tautomer of de-protonated CZA and that for protons bound to aromatic carbon in CZA (CZA1M). The calculated chemical shifts for protons bound to heteroatoms in CZA (7.2 ppm) and in CZA1MA (5.9 ppm) as well as the experimentally detected peaks for protons bound to aromatic carbon (6.2 ppm) and protons bound to heteroatoms (12.1 ppm) for citriazinic acid reportedly located in the similar chemical shift region of the peaks appearing in the spectrum of PCDs.[60, 61] The appearance of these peaks implies that the PCDs comprise pyridinic moieties having chemical structures similar to those of CZA, which has been reported as a molecular fluorophore. The ^{13}C NMR spectrum is shown in Figure S5, compared with the spectrum of the precursor materials (CA and PLys) and osmosis-purified PCDs (0.5–1 kDa for 24 h) (Figure S6). Assignments of peaks for CA and PLys are described in the inserted chemical structure. These peaks were detected at 43.3 ppm, 72.9 ppm, 171.8 ppm, and 175.1 ppm for CA (Figure S5a). Very close to these peaks, sharp, intense peaks at 43.0 ppm, 73.1 ppm, 171.5 ppm, and 174.8 ppm were detected for as-synthesized PCDs (Figure S5c) and those at 43.9 ppm, 72.6 ppm, 172.0 ppm, and 176.0 ppm were detected for osmosis purified PCDs. The presence of these peaks indicates that the CA remains in the PCDs even after osmosis, possibly due to interactions such as hydrogen bonding with amino groups in the polymeric framework from PLys. Sharp, intense peaks appeared at 24.2 ppm (Cγ), 30.4 ppm (Cδ), 36.3 ppm (Cβ), 40.2 ppm (Cε), 56.2 ppm (Cα), and 177.5 ppm (C=O) in ^{13}C NMR spectrum of PLys (Figure S5b), of which the assignments shown in the parentheses are represented as follows; Cγ, Cδ, Cβ: C in alkyl chain, Cε: C in alkyl chain, neighboring amide nitrogen, Cα: C in methine groups, neighboring carbonyl carbon and an amino group.[61] In the ^{13}C NMR spectrum (Figure S5c) of the as-synthesized PCDs, multiple small peaks also appeared. After osmosis purification (Figure S6), some of these small peaks disappeared, leaving the peaks including those at 20-60 ppm, some of which are assigned to alkyl chains in the framework originating from PLys. Those at ~52.8–53.6 ppm were assigned to C having chemical bonding states similar to those of Cα, positions of which may shift due to structural changes such as disordering, fragmentation, and crosslinking or hydrogen bonding of the amino groups with fluorophores. Chemical bonding states

leading to the peak at 84.9 ppm, which is assigned to C in alkynes, those at 113.0 ppm and 147.8 ppm, assigned to C in alkenes or aromatic rings, and that at 160.2 ppm, which is assigned to C in aromatic or pyridinic rings, comprise π and n orbitals possibly contributing to the fluorescence. Additional multiple peaks range from 180-170 ppm peaks corresponding to up-field and down field shift of C=O functional groups indicating intermolecular H-bonding with amide/NH_2 functional groups and esterification/amide bond formation.[62] Pyridinic molecular fluorophores could be entrapped in numerous oligomeric branches possibly via crosslinking or hydrogen bonding in a polymeric framework originating from PLys. Figure S7 shows the comparison of the Raman spectra of PLys and PCDs. Typically, the spectrum of PLys displays Raman-active bands corresponding to the amide bands I, III, the C-C stretching mode, and the methylene bending mode,[63] whereas the spectrum of PCDs additionally comprised a band at 1650–1800 cm^{-1}, in which peaks reportedly assigned to νC=C for protonated forms of CZA via calculation[64] and peaks of νC=O appear, and bands at 1550–1600 cm^{-1} and at 1200–1300 cm^{-1}, in which strong bands have reportedly appeared for CZA in acidic pH.[64] The appearance of these bands for PCDs imply that the presence of chemical structures similar to CZA, which are consistent with the results of the other spectroscopic analyses. The particle hydrodynamic size of PCDs in dispersion was determined as ~5-12 nm (avg. ~5.5 nm) from DLS measurements (Figure 2i). The higher reaction temperature (up to 220 ˚C) did not induce a large change in the hydrodynamic size of PCDs (Figure S8).

Table 2 Total carbon analysis of PCDs compared with commercial graphene oxide.

Sample	Weight of OC	Weight of EC	Weight of total carbon
Graphene oxide	6.3 μg	3.7 μg	10 μg
PCDs	18 μg	Below the detection limit	18 μg

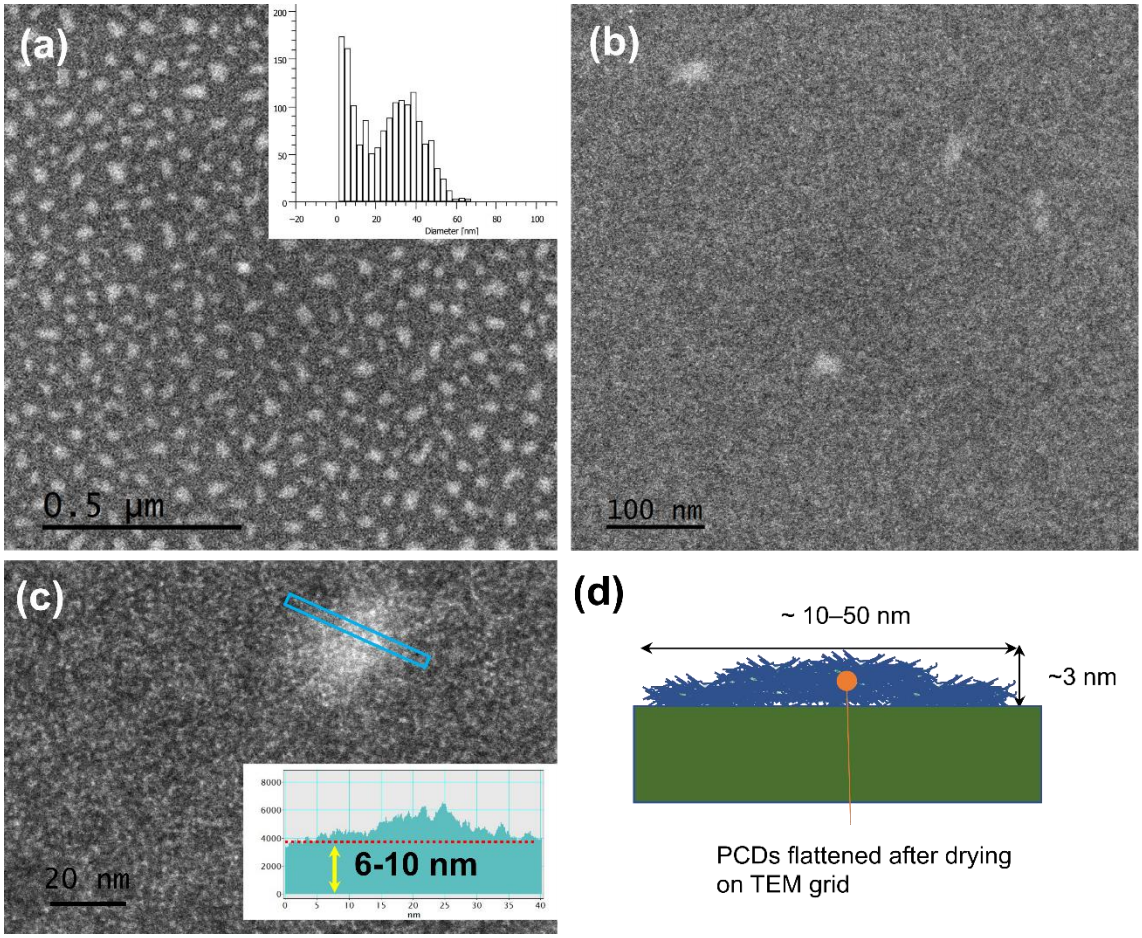

Figure 3. (a and b) TEM grids loaded with PCDs from dispersions with high- and low- concentration, respectively. (c) Determination of PCD height. (d) Proposed schematic representation of flattened PCDs.

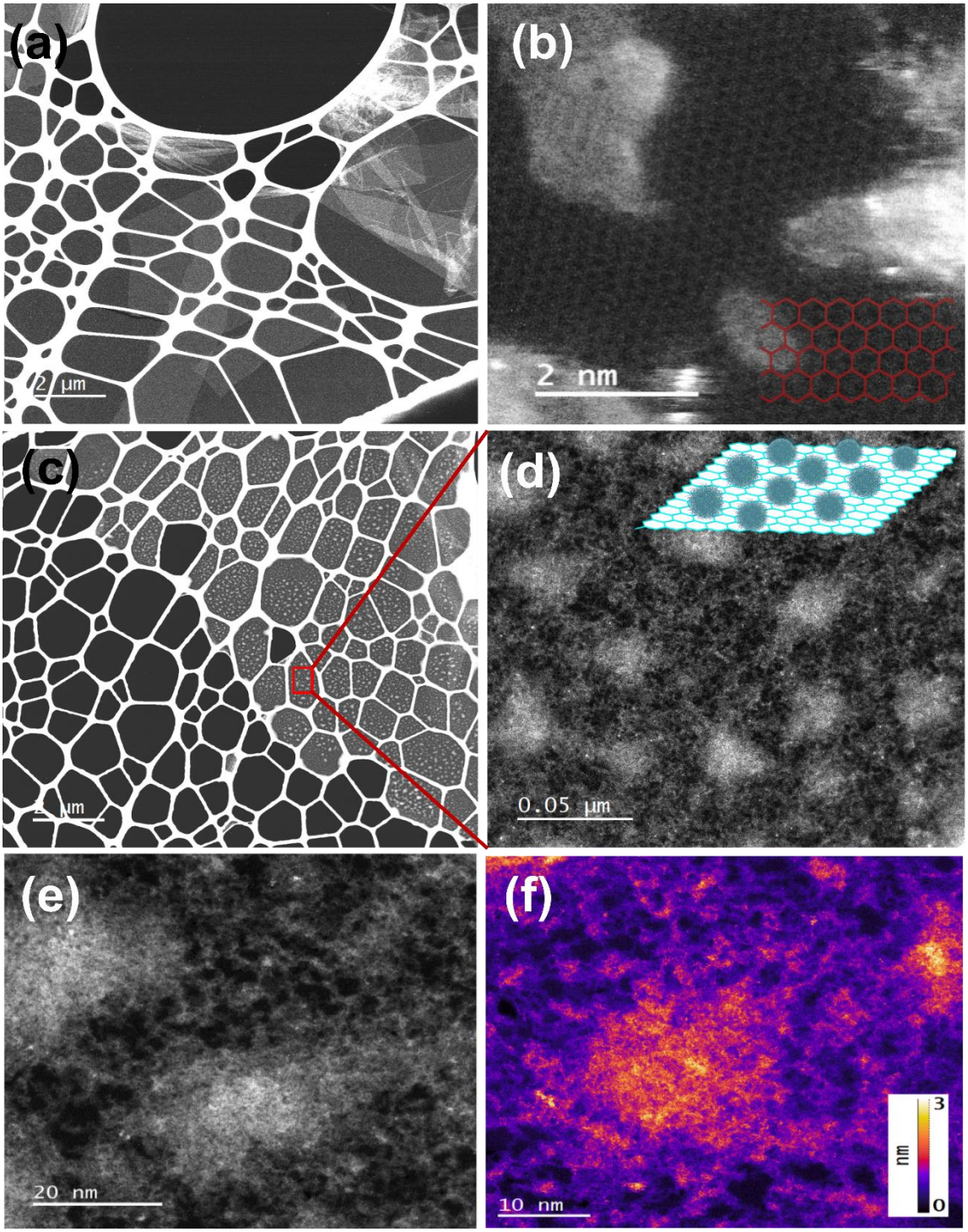

Figure 4. (a) TEM image of monolayer graphene oxide (GO)-coated TEM grid. (b) Atomically clean hexagonal graphene domains. (c-f) Low and high magnification TEM images of PCDs on an atomically thin GO substrate (inset shows the schematic). (e) HR-TEM image of PCDs and (f) height profile of HR-TEM image of PCDs.

To investigate the structure of dried solid forms of PCDs, we employed TEM to observe the PCDs desiccated from dispersions with high (Figure 3.a) and low (Figure 3b) concentration on the TEM grid coated with ultrathin, amorphous C (thickness of C: ~6-10 nm). The TEM image of the grid loaded with PCDs from the high-concentration dispersion accompanied with the histogram (inset) of particle size distributed from the few nm to 60 nm (Figure 3a). A similar particle-size range is also seen for the grid loaded with PCDs from the low-concentration dispersion. The height and width of PCDs is also evaluated from the TEM image of a single PCD (Figure 3c and Figure S9), revealing that the height (~ 3 nm) is smaller and the width (~10 - 65 nm) is larger for PCDs on TEM grid (inset of Figure 3c Figure S9) compared to their hydrodynamic sizes (avg. ~5.5 nm) in aqueous dispersion estimated from DLS. This may be due to flattening during the drying process (Figure 3d), due to their soft polymeric framework. However, the thickness of the amorphous C deposited on the TEM grid is ~ 6-10 nm, which is thicker than typical PCDs; therefore, further detailed structure of PCDs is difficult to investigate using this grid.

To solve this issue, we performed a similar observation on a TEM grid coated with graphene oxide (GO), which is very thin, and which provides low background contrast and is sufficiently flat for observation of PCDs of nano-scale height. Figures 4a and b display TEM and HRTEM images of single-layer GO flakes, which were used to observe PCD structure. The HRTEM image of GO shows the atomically clean domains of hexagonal aromatic rings. Figures 4c and d show the low- and high-magnification images of PCDs on a monolayer GO substrate. The highly magnified TEM image shows the porous, interconnected, close-knit, polymeric PCD framework (Figure 4e). Figure 4.f shows a height profile of PCDs, revealing formation of a porous structure with width of ~10-60 nm and height of ~ 3 nm. These dimensions are respectively larger and smaller than the hydrodynamic size of PCDs in the dispersion, consistent with those of PCDs on the grid coated with amorphous C. Additionally, the topographic images and height profile obtained using AFM also displayed particulate structures with a thickness < 4 nm and width of several tens of nm (Figure S10), which also indicates flattened, aggregated PCDs, as observed with TEM.

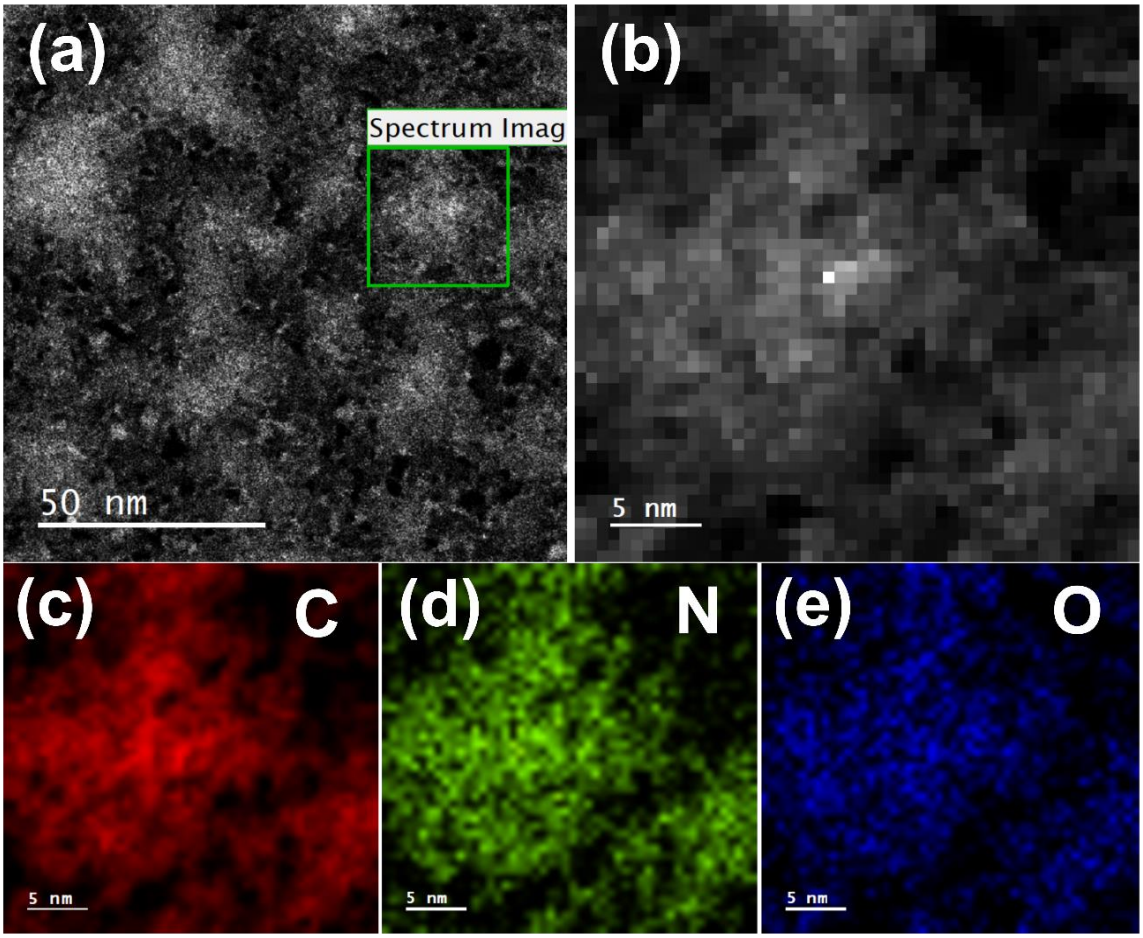

Figure 5. (a) Overview image. (b) ADF-STEM image of a single PCD from the selected region of (a). (c-e) STEM-EELS elemental mapping of C, N, and O atoms from the area in (b).

Figures 5 a and b show a STEM image and an ADF image of single PCD. Figures 5 c-e show elemental mapping of C, N, and O atoms of the corresponding PCD, showing that the chemical composition appears uniform. The distribution of C, N, and O atoms is proportional to the bright regions in ADF images, indicating that they do not originate from grid, but from PCDs, since the grid does not contain N atoms. This STEM-EELS image and ADF mapping of a single PCD reveal that particles appear to have relatively uniform chemical composition and that they appear porous.

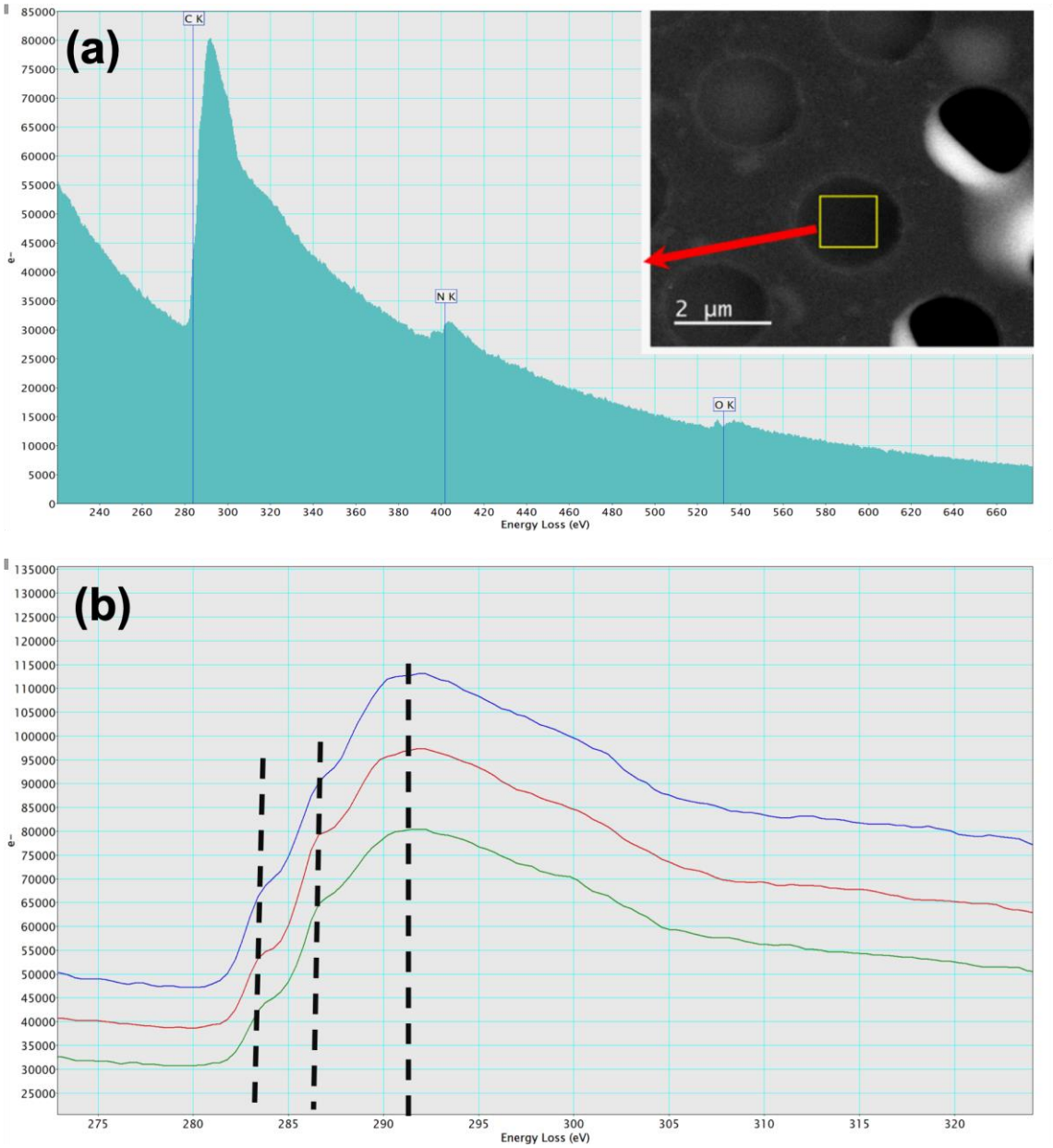

Figure 6. (a) EELS spectrum from suspended region and the inset shows the suspended sample. (b) K-C edge EELS fine feature from different position of the suspended sample.

Chemical composition and bonding nature were evaluated from the EELS spectrum of suspended PCDs in the holes of a C film. Figure 6a shows the EELS spectrum of the suspended sample (inset shows the TEM image of the suspended sample). The EELS spectrum shows the presence of intense peaks of C, O, and N. The average atomic % ratio of C, N, and O are 81.5%, 9.9%, and 8.6 %, respectively. The N/C ratio in the sample is 0.12, which is close to the N/C ratio evaluated by XPS (N/C=0.12) and CHNO analysis (N/C=0.11). For the C K-edge spectrum, there are two peaks located at 284 eV and 292 eV, corresponding to 1s-π* and 1s-σ* electronic transitions, respectively, which

originates from sp^2 bonded carbon. N K-edge and O K-edge spectra also comprise two apparent peaks. Peaks at 397.6 eV and 402 eV correspond to the 1s-π* and 1s-σ* transitions in C=N bonds, respectively. Peaks at 530 eV and 534 eV correspond to the 1s-π* and 1s-σ* transitions in C=O bonds, respectively (Figure 6a).[65-67] Fine features of the near-edge EELS spectrum of C-K (Figure 6.b) show an additional peak at 286.5 eV, attributable to the 1s-π* transition of different O and N-related groups in PCDs.[68-70]

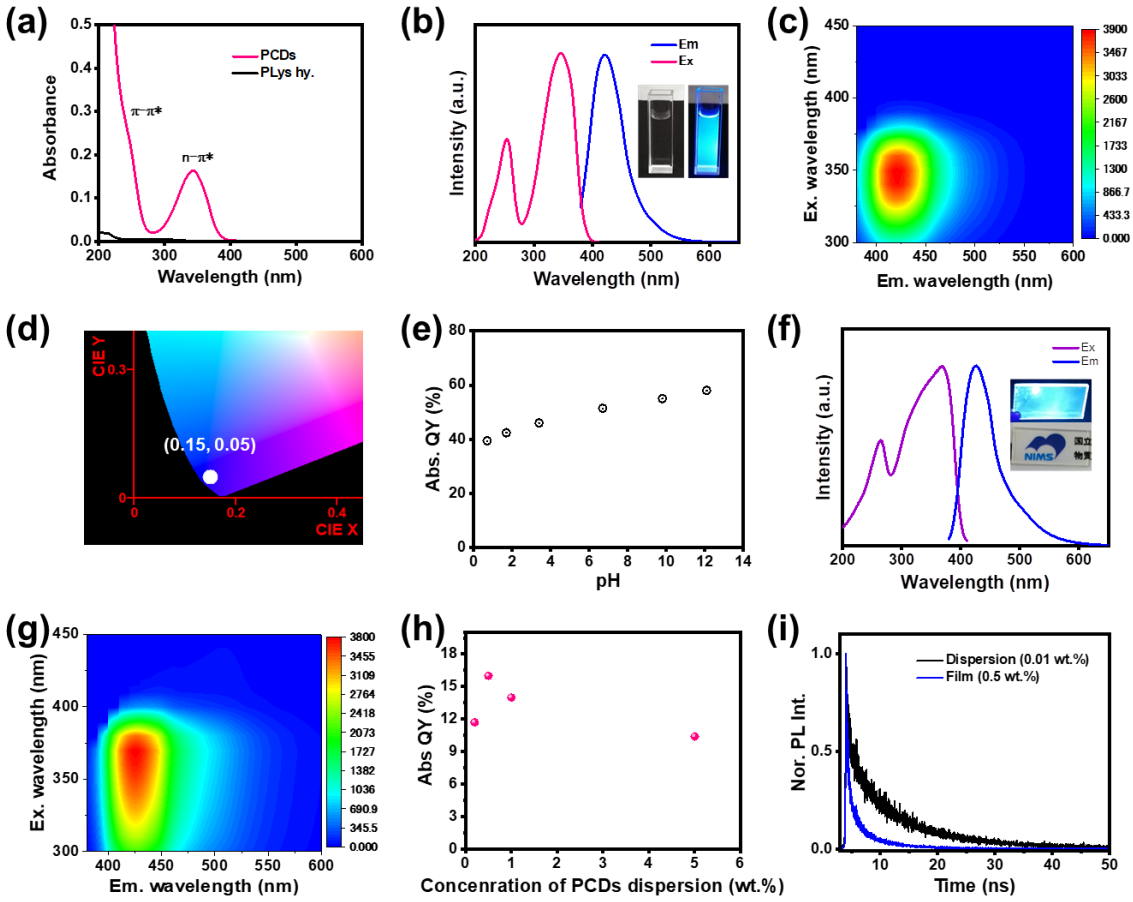

Figure 7. (a) UV-VIS absorbance spectra of PLys and PCDs. (b) PLE and FL spectra of an aqueous dispersion of PCDs (inset shows the photograph of 0.01 wt. % dispersion). (c) 2-D Excitation and emission peaks of an aqueous dispersion. (d) CIE coordinates of the FL spectrum. (e) pH-dependent FL properties of PCDs. (f) PLE and (g) FL and 2-D excitation-emission spectra of a PCD solid film on a quartz substrate. (h) Absolute PLQY value and FL spectra of different PCD films prepared from dispersions of PCDs with different concentration. (i) TRPL spectra of both dispersion and solid film.

The absorption spectrum of PCDs in an aqueous dispersion (Figure 7a) comprises two strong absorption bands at UV-A (344 nm) and UV-C (242 nm) wavelength regions, which are attributable

to n-π* and π-π* transitions in the molecular fluorophores. The n-π* transition originates from excitation of lone pairs in nitrogen atoms at pyridinic sites, whereas the π-π* transition originates from excitation of π orbitals in aromatic rings.[61, 71] Both the UV-A and UV-C absorbance properties of PCDs are drastically enhanced compared to the sample produced by hydrothermal treating of PLys alone. Absorbance of UV-A was enhanced by increasing the reaction temperature (Figure S11), implying that the increase in reaction temperature promotes production of UV-A absorbing aromatic moieties in PCDs. Figure 7b shows the normalized excitation (PLE) and fluorescence (FL) emission spectra of 0.01 wt.% aqueous dispersion, revealing strong absorbance at 344 nm and photoluminescence at 422 nm, respectively. The inset shows a photograph of bright blue emission from a PCD dispersion upon excitation at 365 nm UV. The 2D excitation-emission mapping of the dispersion indicates that PCDs emit blue light (~422 nm) via excitation with UV light and display excitation-independent FL (Figure 7c). The CIE XY chromaticity diagram shows that the (x, y) values of emissions are (0.15, 0.05), indicating the pure blue color emission from PCDs (Figure 7d). An aqueous dispersion of PCDs exhibited an absolute PLQY of 49 % and depends on the pH of the medium. The PLQY of PCD dispersion changes from 40% to 58% when the pH of the medium changes from 0.7 to 12 (Figure 7e). Molecular fluorophores are reportedly non-emissive at low pH values due to protonation.[61] However, PCDs are still emissive with PLQY ~ 40 % at a lower pH. This study strongly suggests that the fluorophores cannot be protonated because they are already H-bonded with the polymeric framework. Typically, luminescence of CDs is quenched in the solid state, i.e., after they are dried to cause agglomeration, because self-absorption results from the close spacing. Interestingly, PCDs in the present study exhibited non-quenched strong emission even in the dried solid state (Figure S12). Figure 7f shows PLE and FL properties of a transparent smooth film on a quartz substrate. The film also exhibited strong UV-A absorbance and emission of blue light centered at 425 nm. The inset of Figure 7f shows a transparent film and its blue-light emission via excitation at 365 nm. PCDs in a solid film also exhibited excitation-independent FL similar to that of PCDs in the dispersion, exhibiting an emission peak centered at 425 nm (Figure 7g). Figure 7h shows a comparison of PLQY and FL spectra of films prepared from dispersions of PCDs with different concentrations. Films were prepared from 0.5 wt.% PCD dispersion exhibited solid-state emission and films prepared from the dispersion with increased concentration exhibited decreased PLQY, indicating that self-absorption was promoted (Figure 7h). As a result, the PLQY of PCDs in a solid state is ~16 %, far lower than its aqueous dispersion (~49 %). Stability of PCDs in dispersion and solid-state was further investigated. Free-molecular fluorophores are reportedly not stable in aqueous medium and drastically decrease in PLQY after a few days.[31] These PCDs are stable in aqueous dispersion and did not show decreased PLQY even after a few days (Figure S13). The PLQY of PCDs both in dispersions and thin films was also stable even after long exposure to UV-A radiation (365 nm, 4 mW UV power for 2 h), maintaining ~90 % PL intensity (Figure S14). The slight decrease in PLQY may be due to

photobleaching. Overall, these PCDs are stable, which may be due to protection of fluorophores inside the polymer matrix. Figure 7i shows the time-resolved photoluminescence (TRPL) spectrum of both aqueous dispersion and solid transparent film. The average PL lifetime (τ_{avg}) was obtained from the bi-exponential fitted time decay spectra using the following equation: $\tau_{avg} = (A_1 \tau^2_1 + A_2 \tau^2_2)/(A_1\tau_1 + A_2\tau_2)$, where A_1, and A_2 are the amplitudes, and τ_1 and τ_2 are the PL decay times.[72] The obtained values of A_1, A_2, τ_1, and τ_1 is summarized in Table-S2. The decay time of excited electrons of the film (τ_{avg}: 1.1 ns) was shorter than that of the dispersion (τ_{avg}: 7.63 ns) due to enhancement of non-radiative recombination transition in the film compared to the dispersion (Figure S15). As a result, a decrease in the PLQY from colloidal dispersion to solid film is observed.[61] Overall, these PCDs can directly be used as a transparent pure blue light emitter in solid-state. This is due to the presence of the matrix, which keeps emission centers well separated, even in a dried, solid state.

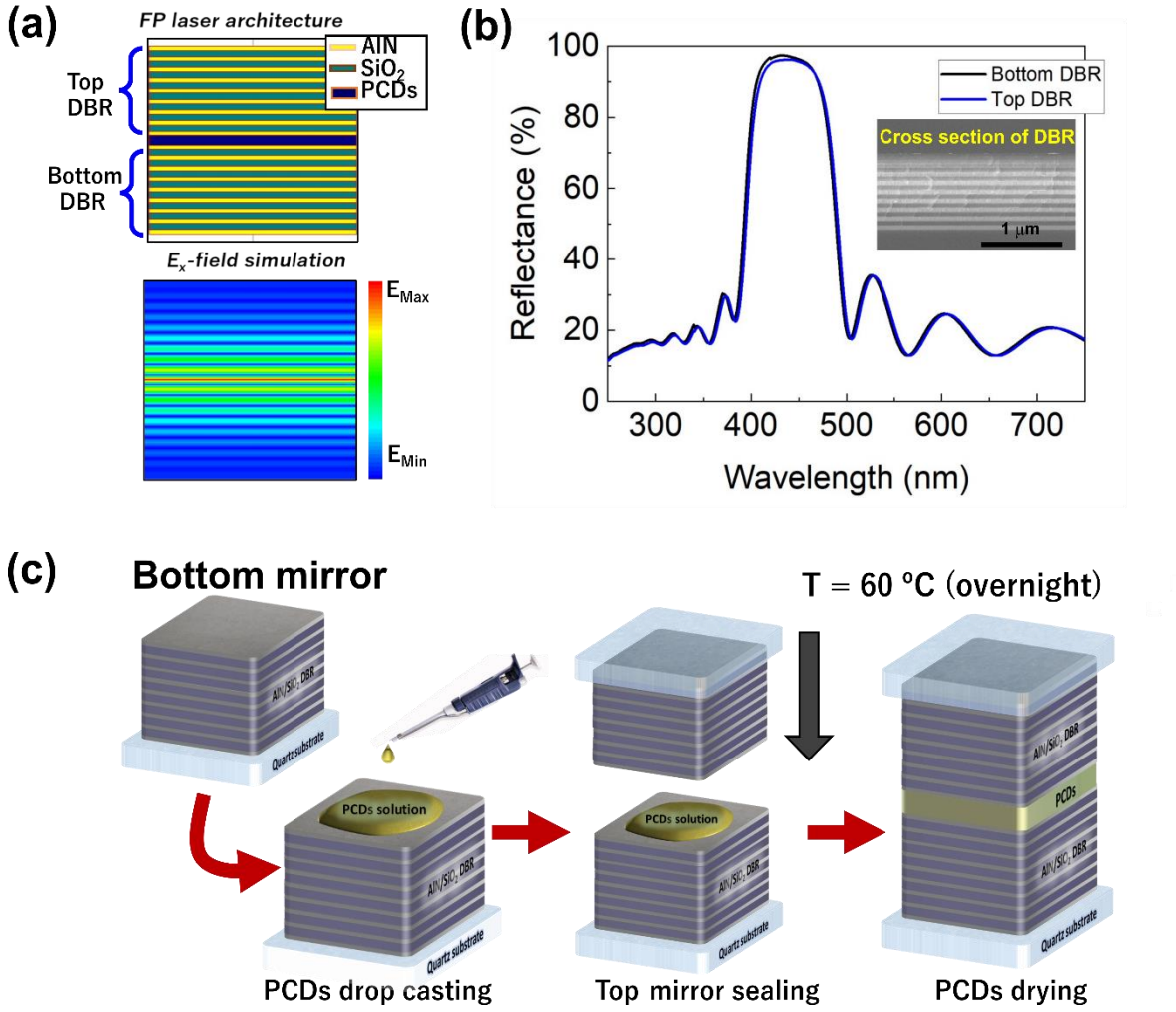

Figure 8. Fabry-Pérot (FP) laser architecture by sandwiching PCDs as gain media and electric field simulation of confinement of emitted light by DBR microcavity. (b) Reflectance spectra and inset show a cross-sectional SEM image of sputtered DBR mirror. (c) Schematic representation of fabrication steps to obtain a quartz/DBR/PCDs/DBR/quartz sample for optical gain experiments.

PCDs exhibit good self-quenching resistant, solid-state emission with nanosecond PL lifetime (Figures 7 f and i). These properties are very attractive for optical amplification processes, and in this context, we carried out laser experiments utilizing synthetized PCDs as gain media. With this aim, a Fabry-Pérot (FP) laser architecture was fabricated by sandwiching a PCD layer between two semi-transparent DBRs specifically designed for PCDs (Figure 8 a) and the electric field simulation shows confinement of emitted light by top and bottom FP based DBR microcavity. In order to achieve optical amplification of PCD emission, DBR mirrors were engineered to yield high reflectance (R > 95%) in the main emission spectral range of PCDs (400-480 nm), while simultaneously allowing UV

transmittance (T ~80% @355 nm) to reach PCDs for efficient excitation (Figure 8.a). Since materials with high energy band gaps exhibit high transparency at 355 nm, alternating layers of AlN and SiO_2 were deposited via magnetron sputtering on quartz substrates, acting as DBR mirrors to constitute the optical resonators. Figure 8b inset shows a SEM cross-sectional image of one of the fabricated DBR structures. Optical properties of these photonic structures are related to the refractive index contrast between the constituent materials and the thickness of each layer. Prior to deposition, optical simulations of AlN-SiO_2 DBR resonators were carried out using RCWA to ensure the appropriate spectral response of the resonators for PCDs. The final PCD samples for optical gain experiments were prepared as depicted in Figure 8c. 10 µL of 20.6 wt.% PCD dispersion was drop-casted on the surface of one of the sputtered DBR mirrors and immediately sandwiched with an upside-down DBR mirror to ensure small cavity lengths and smooth interfaces. The Quartz/DBR/PCDs/DBR/Quartz sample was dried at 60ºC overnight to complete solidification of the PCD layer.

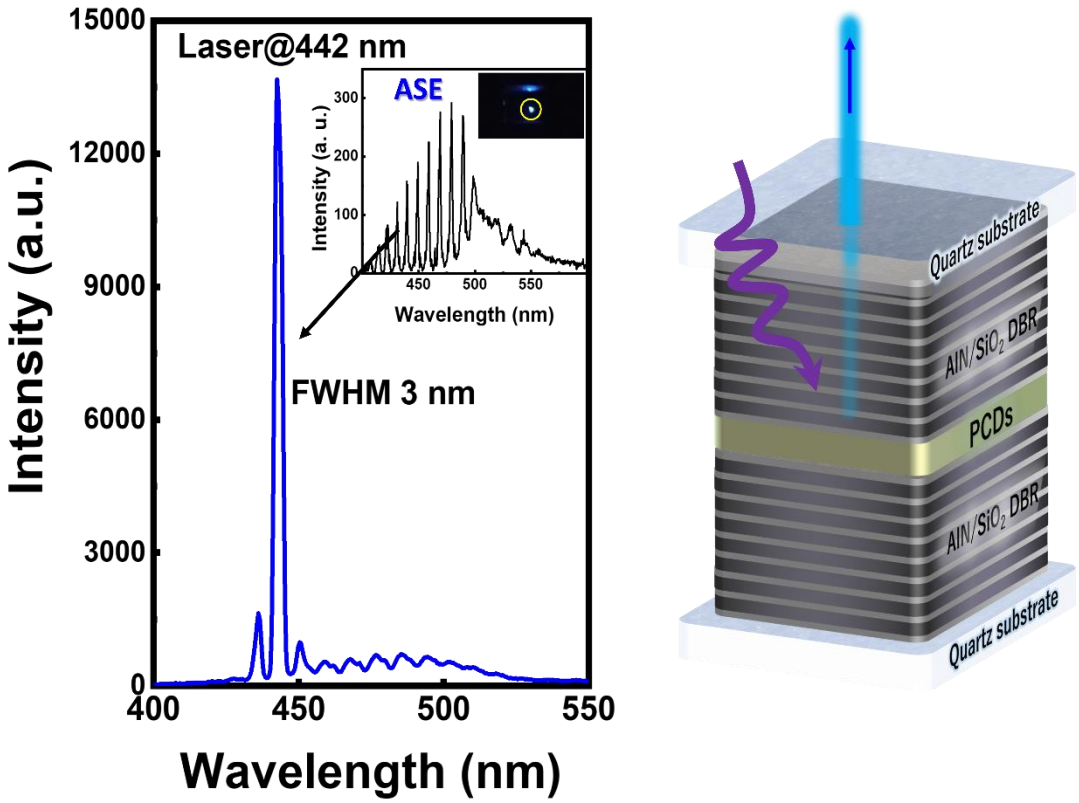

Figure 9. Laser emission at a wavelength matching the maximum emission of PCDs. Inset shows the Amplified Spontaneous Emission (ASE) of the quartz/DBR/PCDs/DBR/quartz sample upon UV excitation, as well as a photograph of the sample during the experiments. A schematic representation of the laser emission is included at the right side of Figure 9.

After drying, the sample was placed on a custom-made optical microscopy system and was subjected to UV radiation (λ = 355 nm). Experiments were performed in back-scattering configuration, with both excitation and emission performed at normal incidence. At low excitation power, the competition of longitudinal modes for available optical gain results in many sharp emission peaks, corresponding to an amplified spontaneous emission (ASE) regime. In contrast with other luminescent systems devoid of photonic microcavities,[73, 74] since this regime is achieved even at very low excitation powers, no transition from spontaneous emission to ASE is observed. A recorded ASE spectrum is shown in the inset of Figure 9. As observed, the ASE follows the spectral response of the DBR mirrors as a result of photonic coupling of PCD emission and localized electromagnetic modes from the DBR resonator in the high-reflectance spectral range from 400 -500 nm. Weaker amplification features are also observed at longer wavelengths, in accordance with lower gain provided by lower reflectance values of the DBR resonator at these wavelengths. The ASE intensity of PCDs increases linearly with incident pump power until laser regime is finally achieved. The transition from ASE to laser regime is characterized by an abrupt increase of the intensity of the longitudinal mode with the highest optical gain. This ASE to laser transition indicates the laser threshold, which is observed at a pump power density of approximately 1.6 kW/cm^2, which is comparable to other reported CD-based laser systems, mostly ranging from 0.07 to 220 kW/cm^2.[75-78] Figure 9 shows an example of blue laser emission measured at a wavelength of λ = 442 nm yielding ~ 45 times higher intensity than the emitted ASE radiation (Figure 9, inset). Unfortunately, the laser amplification process involves intense localized photon densities that cause thermal damage to the PCD layer. For this reason, laser emission remains unstable and no input-output power curves could be measured. Nevertheless, the results hold promise for fabrication of biodegradable optical amplifier devices based on novel polymeric gain media.

Conclusions

A new type of pure blue light-emitting PCDs has been synthesized in colloidal and solid state via the hydrothermal reaction from natural, biodegradable ingredients (CA, PLys). Synthesized PCDs had hydrodynamic sizes in aqueous dispersion ranging from 4 to 10 nm (avg. ~5.5 nm) and exhibited an absolute PLQY up to 49 %. STEM-EELS observations revealed internal structures of PCDs, including compositional gradients and elemental distribution as well as diameters and thicknesses of PCDs deposited on the grid. In combination with NMR, XPS, vibrational analyses, and total carbon analysis, we propose a structure composed of tiny clusters with uniform element distribution, which has an organic polymer framework embracing fluorescent aromatic moieties that do not contain graphitic inorganic carbon, leading to soft organic polymeric characteristics and excellent self-quenching resistance in solid form. Spectroscopic analyses also identify aromatic moieties with π-conjugation, which may act as photoluminescent centers that emit radiatively. To exploit PCD-suppressed self-quenching and lifetimes on the order of nanoseconds, optical gain experiments were also carried out. We prepared photonic planar

microcavities formed of two DBRs that sandwich PCDs. Both sharp ASE and unstable single-mode laser emission are achieved. These results indicate the structural and optical properties of hydrothermally produced PCDs, and may pave the way for development of completely rare-earth-free, light-emitting, and other photonic devices.

ASSOCIATED CONTENT

Supporting Information

The following files are available free of charge.

^{1}H and ^{13}C NMR spectra, CHNO elemental analysis, TEM images, Raman spectra, DLS, UV-Vis spectra, PL stability, Time-Resolved Photoluminescence (TRPL).

AUTHOR INFORMATION

Corresponding Authors

Barun Kumar Barman -International Center for Materials Nanoarchitectonics (WPI-MANA), National Institute for Materials Science (NIMS), Tsukuba, Ibaraki 305-0044, Japan; orcid.org/0000-0002-9894-1890

Email: BARMAN.Kumarbarun@nims.go.jp (B.K.B.)

David Hernández-Pinilla -International Center for Materials Nanoarchitectonics (WPI-MANA), National Institute for Materials Science (NIMS), Tsukuba, Ibaraki 305-0044, Japan; orcid.org/0000-0002-9242-7495.
Email: mayphys87@gmail.com (D.-H. P)

Riichiro Ohta- L'Oréal Research and Innovation, KSP R&D, 3-2-1 Sakado, Takatsu-ku, Kawasaki, Kanagawa 213-0012, Japan; orcid.org/0000-0003-2386-9721.
Email: riichiro.ohta@loreal.com (R.O)

Tadaaki Nagao – International Center for Materials Nanoarchitectonics (WPI-MANA), National Institute for Materials Science (NIMS), Tsukuba, Ibaraki 305-0044, Japan;

Department of Condensed Matter Physics, Hokkaido University, Sapporo, Hokkaido 060-0810, Japan; orcid.org/0000- 0002-6746-2686

Email: NAGAO.Tadaaki@nims.go.jp (T.N.)

Authors

Barun Kumar Barman -International Center for Materials Nanoarchitectonics (WPI-MANA), National Institute for Materials Science (NIMS), Tsukuba, Ibaraki 305-0044, Japan; orcid.org/0000-0002-9894-1890.

David Hernández-Pinilla -International Center for Materials Nanoarchitectonics (WPI-MANA), National Institute for Materials Science (NIMS), Tsukuba, Ibaraki 305-0044, Japan; orcid.org/0000-0002-9242-7495.

Ovidiu Cretu-Electron Microscopy Group, National Institute for Materials Science (NIMS), Tsukuba, Ibaraki 305-0044, Japan; orcid.org/0000-0002-1822-8172.

Riichiro Ohta- L'Oréal Research and Innovation, KSP R&D, 3-2-1 Sakado, Takatsu-ku, Kawasaki, Kanagawa 213-0012, Japan; orcid.org/0000-0003-2386-9721.
Email: riichiro.ohta@rd.loreal.com (R.O)

Keiko Okano - International Center for Materials Nanoarchitectonics (WPI-MANA), National Institute for Materials Science (NIMS), Tsukuba, Ibaraki 305-0044, Japan

Toshifumi Shiroya- L'Oréal Research and Innovation, KSP R&D, 3-2-1 Sakado, Takatsu-ku, Kawasaki, Kanagawa 213-0012, Japan

Jun Sasai- L'Oréal Research and Innovation, KSP R&D, 3-2-1 Sakado, Takatsu-ku, Kawasaki, Kanagawa 213-0012, Japan

Koji Kimoto- Electron Microscopy Group, National Institute for Materials Science (NIMS), Tsukuba, Ibaraki 305-0044, Japan; orcid.org/0000-0002-3927-0492.

Tadaaki Nagao – International Center for Materials Nanoarchitectonics (WPI-MANA), National Institute for Materials Science (NIMS), Tsukuba, Ibaraki 305-0044, Japan;

Department of Condensed Matter Physics, Hokkaido University, Sapporo, Hokkaido 060-0810, Japan; orcid.org/0000- 0002-6746-2686.

ACKNOWLEDGMENTS

This work was financially supported by the L'Oréal-NIMS collaboration program. BKB and DHP acknowledge "The Japan Society for the Promotion of Science (JSPS)" for a JSPS postdoctoral fellowship. The authors also acknowledge Dr. Hidehiko Asanuma for fruitful discussions and Dr. Hiroyuki Yamada for AFM imaging and analysis. Authors also thank the Namiki foundry at NIMS for XRD, UV, FL, and optical characterizations, and Sumika Chemical Analysis Service, Ltd. for total carbon analysis. Authors also acknowledge Showa Denko Materials Techno Service Co., Ltd. for ^{1}H, ^{13}C NMR measurements and peak assignments.

CONFLICTS OF INTEREST

The authors declare no conflicts of interest.

References

1. Bourlinos, A. B.; Stassinopoulos, A.; Anglos, D.; Zboril, R.; Georgakilas, V.; Giannelis, E. P., Photoluminescent Carbogenic Dots. *Chemistry of Materials* **2008,** *20* (14), 4539-4541.

2. Hu, C.; Li, M.; Qiu, J.; Sun, Y.-P., Design and fabrication of carbon dots for energy conversion and storage. *Chemical Society Reviews* **2019,** *48* (8), 2315-2337.

3. Liu, J.; Geng, Y.; Li, D.; Yao, H.; Huo, Z.; Li, Y.; Zhang, K.; Zhu, S.; Wei, H.; Xu, W.; Jiang, J.; Yang, B., Deep Red Emissive Carbonized Polymer Dots with Unprecedented Narrow Full Width at Half Maximum. *Advanced Materials* **2020,** *32* (17), 1906641.

4. Liu, J.; Li, R.; Yang, B., Carbon Dots: A New Type of Carbon-Based Nanomaterial with Wide Applications. *ACS Central Science* **2020,** *6* (12), 2179-2195.

5. Sadhanala, H. K.; Nanda, K. K., Boron and Nitrogen Co-doped Carbon Nanoparticles as Photoluminescent Probes for Selective and Sensitive Detection of Picric Acid. *The Journal of Physical Chemistry C* **2015,** *119* (23), 13138-13143.

6. Semeniuk, M.; Yi, Z.; Poursorkhabi, V.; Tjong, J.; Jaffer, S.; Lu, Z.-H.; Sain, M., Future Perspectives and Review on Organic Carbon Dots in Electronic Applications. *ACS Nano* **2019,** *13* (6), 6224-6255.

7. Sun, Y.-P.; Zhou, B.; Lin, Y.; Wang, W.; Fernando, K. A. S.; Pathak, P.; Meziani, M. J.; Harruff, B. A.; Wang, X.; Wang, H.; Luo, P. G.; Yang, H.; Kose, M. E.; Chen, B.; Veca, L. M.; Xie, S.-Y., Quantum-Sized Carbon Dots for Bright and Colorful Photoluminescence. *Journal of the American Chemical Society* **2006,** *128* (24), 7756-7757.

8. Xu, X.; Ray, R.; Gu, Y.; Ploehn, H. J.; Gearheart, L.; Raker, K.; Scrivens, W. A., Electrophoretic Analysis and Purification of Fluorescent Single-Walled Carbon Nanotube Fragments. *Journal of the American Chemical Society* **2004,** *126* (40), 12736-12737.

9. Yan, Y.; Gong, J.; Chen, J.; Zeng, Z.; Huang, W.; Pu, K.; Liu, J.; Chen, P., Recent Advances

on Graphene Quantum Dots: From Chemistry and Physics to Applications. *Advanced Materials* **2019,** *31* (21), 1808283.

10. Nie, H.; Li, M.; Li, Q.; Liang, S.; Tan, Y.; Sheng, L.; Shi, W.; Zhang, S. X.-A., Carbon Dots with Continuously Tunable Full-Color Emission and Their Application in Ratiometric pH Sensing. *Chemistry of Materials* **2014,** *26* (10), 3104-3112.

11. Sk, M. A.; Ananthanarayanan, A.; Huang, L.; Lim, K. H.; Chen, P., Revealing the tunable photoluminescence properties of graphene quantum dots. *Journal of Materials Chemistry C* **2014,** *2* (34), 6954-6960.

12. Tetsuka, H.; Asahi, R.; Nagoya, A.; Okamoto, K.; Tajima, I.; Ohta, R.; Okamoto, A., Optically Tunable Amino-Functionalized Graphene Quantum Dots. *Advanced Materials* **2012,** *24* (39), 5333-5338.

13. Wang, Y.; Kalytchuk, S.; Zhang, Y.; Shi, H.; Kershaw, S. V.; Rogach, A. L., Thickness-Dependent Full-Color Emission Tunability in a Flexible Carbon Dot Ionogel. *The Journal of Physical Chemistry Letters* **2014,** *5* (8), 1412-1420.

14. Zhu, S.; Song, Y.; Zhao, X.; Shao, J.; Zhang, J.; Yang, B., The photoluminescence mechanism in carbon dots (graphene quantum dots, carbon nanodots, and polymer dots): current state and future perspective. *Nano Research* **2015,** *8* (2), 355-381.

15. Barman, B. K.; Okano, K.; Deguchi, K.; Ohki, S.; Hashi, K.; Goto, A.; Nagao, T., N-Dopant Site Formulation for White-Light-Emitting Carbon Dots with Tunable Chromaticity. *ACS Sustainable Chemistry & Engineering* **2022,** *10* (49), 16136-16149.

16. Jiang, K.; Sun, S.; Zhang, L.; Lu, Y.; Wu, A.; Cai, C.; Lin, H., Red, Green, and Blue Luminescence by Carbon Dots: Full-Color Emission Tuning and Multicolor Cellular Imaging. *Angewandte Chemie International Edition* **2015,** *54* (18), 5360-5363.

17. Krysmann, M. J.; Kelarakis, A.; Dallas, P.; Giannelis, E. P., Formation Mechanism of Carbogenic Nanoparticles with Dual Photoluminescence Emission. *Journal of the American Chemical Society* **2012,** *134* (2), 747-750.

18. Lin, L.; Zhang, S., Creating high yield water soluble luminescent graphene quantum dots via exfoliating and disintegrating carbon nanotubes and graphite flakes. *Chemical Communications* **2012,** *48* (82), 10177-10179.

19. Miao, X.; Qu, D.; Yang, D.; Nie, B.; Zhao, Y.; Fan, H.; Sun, Z., Synthesis of Carbon Dots with Multiple Color Emission by Controlled Graphitization and Surface Functionalization. *Advanced Materials* **2018,** *30* (1), 1704740.

20. Yoon, H.; Chang, Y. H.; Song, S. H.; Lee, E.-S.; Jin, S. H.; Park, C.; Lee, J.; Kim, B. H.; Kang, H. J.; Kim, Y.-H.; Jeon, S., Intrinsic Photoluminescence Emission from Subdomained Graphene Quantum Dots. *Advanced Materials* **2016,** *28* (26), 5255-5261.

21. Zhu, S.; Wang, L.; Zhou, N.; Zhao, X.; Song, Y.; Maharjan, S.; Zhang, J.; Lu, L.; Wang, H.; Yang, B., The crosslink enhanced emission (CEE) in non-conjugated polymer dots: from the photoluminescence mechanism to the cellular uptake mechanism and internalization. *Chemical Communications* **2014,** *50* (89), 13845-13848.

22. He, F.; Bai, J.; Cheng, Y.; Weerasinghe, K.; Meng, X.; Xu, H.; Zhang, W.; Fang, X.; Li, H.-B.; Ding, T., Insights into Fluorophores of Dual-Emissive Carbon Dots Derived by Naphthalenediol Solvothermal Synthesis. *The Journal of Physical Chemistry C* **2021,** *125* (9), 5207-5216.

23. He, F.; Li, H.-B.; Xu, H.; Bai, J.; Cheng, Y.; Meng, X.; Zhang, W.; Fang, X.; Xu, Y.; Ding, T., ESIPT fluorophores derived from 2,3-dichloro-5,6-dicyano-p-benzoquinone based carbon dots for dual emission and multiple anti-counterfeiting. *Physical Chemistry Chemical Physics* **2021,** *23* (1), 388-398.

24. Meng, X.; Wang, Y.; Liu, X.; Wang, M.; Zhan, Y.; Liu, Y.; Zhu, W.; Zhang, W.; Shi, L.; Fang, X., Supramolecular nanodots derived from citric acid and beta-amines with high quantum yield and sensitive photoluminescence. *Opt Mater* **2018,** *77*, 48-54.

25. Barman, B. K.; Sele Handegård, Ø.; Hashimoto, A.; Nagao, T., Carbon Dot/Cellulose-Based Transparent Films for Efficient UV and High-Energy Blue Light Screening. *ACS Sustainable Chemistry & Engineering* **2021,** *9* (29), 9879-9890.

26. Zhu, S.; Zhao, X.; Song, Y.; Lu, S.; Yang, B., Beyond bottom-up carbon nanodots: Citric-acid derived organic molecules. *Nano Today* **2016,** *11* (2), 128-132.

27. Tao, S.; Zhou, C.; Kang, C.; Zhu, S.; Feng, T.; Zhang, S.-T.; Ding, Z.; Zheng, C.; Xia, C.; Yang, B., Confined-domain crosslink-enhanced emission effect in carbonized polymer dots. *Light: Science & Applications* **2022,** *11* (1), 56.

28. Vallan, L.; Urriolabeitia, E. P.; Ruipérez, F.; Matxain, J. M.; Canton-Vitoria, R.; Tagmatarchis, N.; Benito, A. M.; Maser, W. K., Supramolecular-Enhanced Charge Transfer within Entangled Polyamide Chains as the Origin of the Universal Blue Fluorescence of Polymer Carbon Dots. *Journal of the American Chemical Society* **2018,** *140* (40), 12862-12869.

29. Tao, S.; Zhu, S.; Feng, T.; Zheng, C.; Yang, B., Crosslink-Enhanced Emission Effect on Luminescence in Polymers: Advances and Perspectives. *Angewandte Chemie International Edition* **2020,** *59* (25), 9826-9840.

30. Kasprzyk, W.; Świergosz, T.; Bednarz, S.; Walas, K.; Bashmakova, N. V.; Bogdał, D., Luminescence phenomena of carbon dots derived from citric acid and urea – a molecular insight. *Nanoscale* **2018,** *10* (29), 13889-13894.

31. Song, Y.; Zhu, S.; Zhang, S.; Fu, Y.; Wang, L.; Zhao, X.; Yang, B., Investigation from chemical structure to photoluminescent mechanism: a type of carbon dots from the pyrolysis of citric acid and an amine. *Journal of Materials Chemistry C* **2015,** *3* (23), 5976-5984.

32. Yang, W.; Liu, F.; Li, R.; Wang, X.; Hao, W., Multiple Stimuli-Responsive Fluorescent Sensor from Citric Acid and 1-(2-Aminoethyl)piperazine. *Acs Appl Mater Inter* **2018,** *10* (10), 9123-9128.

33. Geng, T.; Feng, T. L.; Ma, Z. W.; Cao, Y.; Chen, Y. P.; Tao, S. Y.; Xiao, G. J.; Lu, S. Y.; Yang, B.; Zou, B., Insights into supramolecular-interaction-regulated piezochromic carbonized polymer dots. *Nanoscale* **2019,** *11* (11), 5072-5079.

34. Huo, Z. P.; Chen, G.; Geng, Y. J.; Cong, L. L.; Pan, L. Y.; Xu, W. Q.; Xu, S. P., A two-photon fluorescence, carbonized polymer dot (CPD)-based, wide range pH nanosensor: a view from the surface state. *Nanoscale* **2020,** *12* (16), 9094-9103.

35. Li, F.; Wang, X.; Liu, W.; Wang, L. Q.; Wang, G. Y., One-step solvothermal synthesis of red emissive carbonized polymer dots for latent fingerprint imaging. *Opt Mater* **2018,** *86*, 79-86.

36. Li, P.; Xue, S.; Sun, L.; Zong, X.; An, L.; Qu, D.; Wang, X.; Sun, Z., Formation and fluorescent mechanism of red emissive carbon dots from o-phenylenediamine and catechol system. *Light: Science & Applications* **2022,** *11* (1), 298.

37. Liu, J. J.; Geng, Y. J.; Li, D. W.; Yao, H.; Huo, Z. P.; Li, Y. F.; Zhang, K.; Zhu, S. J.; Wei, H. T.; Xu, W. Q.; Jiang, J. L.; Yang, B., Deep Red Emissive Carbonized Polymer Dots with Unprecedented Narrow Full Width at Half Maximum. *Advanced Materials* **2020,** *32* (17).

38. Liu, J. J.; Li, D. W.; Zhang, K.; Yang, M. X.; Sun, H. C.; Yang, B., One-Step Hydrothermal Synthesis of Nitrogen-Doped Conjugated Carbonized Polymer Dots with 31% Efficient Red Emission for In Vivo Imaging. *Small* **2018,** *14* (15).

39. Lu, S. Y.; Sui, L. Z.; Wu, M.; Zhu, S. J.; Yong, X.; Yang, B., Graphitic Nitrogen and High-Crystalline Triggered Strong Photoluminescence and Room-Temperature Ferromagnetism in Carbonized Polymer Dots. *Adv Sci* **2019,** *6* (2).

40. Ru, Y.; Ai, L.; Jia, T. T.; Liu, X. J.; Lu, S. Y.; Tang, Z. Y.; Yang, B., Recent advances in chiral carbonized polymer dots: From synthesis and properties to applications. *Nano Today* **2020,** *34*.

41. Song, Y.; Zhu, S.; Shao, J.; Yang, B., Polymer carbon dots—a highlight reviewing their unique structure, bright emission and probable photoluminescence mechanism. *Journal of Polymer Science Part A: Polymer Chemistry* **2017,** *55* (4), 610-615.

42. Tan, C. L.; Zhou, C.; Peng, X. Y.; Zhi, H. Z.; Wang, D.; Zhan, Q. Q.; He, S. L., Sulfuric Acid Assisted Preparation of Red-Emitting Carbonized Polymer Dots and the Application of Bio-lmaging. *Nanoscale Res Lett* **2018,** *13*.

43. Tao, S.; Zhu, S.; Feng, T.; Xia, C.; Song, Y.; Yang, B., The polymeric characteristics and photoluminescence mechanism in polymer carbon dots: A review. *Materials Today Chemistry* **2017,** *6*, 13-25.

44. Wang, Z. F.; Liu, Y.; Zhen, S. J.; Li, X. X.; Zhang, W. G.; Sun, X.; Xu, B. Y.; Wang, X.; Gao, Z. H.; Meng, X. G., Gram-Scale Synthesis of 41% Efficient Single-Component White-Light-Emissive Carbonized Polymer Dots with Hybrid Fluorescence/Phosphorescence for White Light-Emitting Diodes. *Adv Sci* **2020,** *7* (4).

45. Xia, C. L.; Zhu, S. J.; Feng, T. L.; Yang, M. X.; Yang, B., Evolution and Synthesis of Carbon Dots: From Carbon Dots to Carbonized Polymer Dots. *Adv Sci* **2019,** *6* (23).

46. Xia, C. L.; Zhu, S. J.; Zhang, S. T.; Zeng, Q. S.; Tao, S. Y.; Tian, X. Z.; Li, Y. F.; Yang, B., Carbonized Polymer Dots with Tunable Room-Temperature Phosphorescence Lifetime and Wavelength. *Acs Appl Mater Inter* **2020,** *12* (34), 38593-38601.

47. Zhao, X. H.; Li, J.; Liu, D. N.; Yang, M. X.; Wang, W. J.; Zhu, S. J.; Yang, B., Self-Enhanced Carbonized Polymer Dots for Selective Visualization of Lysosomes and Real-Time Apoptosis Monitoring. *Iscience* **2020,** *23* (4).

48. Zhao, Y.; Zeng, Q. S.; Yu, Y.; Feng, T. L.; Zhao, Y. J.; Wang, Z. D.; Li, Y.; Liu, C. M.; Liu,

J. J.; Wei, H. T.; Zhu, S. J.; Kang, Z. H.; Zhang, H.; Yang, B., Enhanced charge separation and photocatalytic hydrogen evolution in carbonized-polymer-dot-coupled lead halide perovskites. *Mater Horiz* **2020,** *7* (10), 2719-2725.

49. Lv, K.-P.; Norman, L.; Li, Y.-L., Restrictions on the Production of Multi-Wall Carbon Nanotubes and Nanofibers by Gallionella sp. *Geomicrobiology Journal* **2016,** *33* (8), 709-715.

50. Yajima, A.; Abe, S.; Fuse, T.; Mera, Y.; Maeda, K.; Suzuki, K., Electron-Irradiation-Induced Ordering In Tetrahedral-Amorphous Carbon Films. *Molecular Crystals and Liquid Crystals* **2002,** *388* (1), 147-151.

51. Ogura, I., *Guide to Evaluating Emission and Exposure of Carbon Nanomaterials (carbon nanotubes and graphenes)*. 2018.

52. Suwalsky, M.; Llanos, A., An X-ray diffraction study of poly(L-lysine hydrobromide). *Biopolymers* **1977,** *16* (2), 403-413.

53. Yang, Z.; Xu, M.; Liu, Y.; He, F.; Gao, F.; Su, Y.; Wei, H.; Zhang, Y., Nitrogen-doped, carbon-rich, highly photoluminescent carbon dots from ammonium citrate. *Nanoscale* **2014,** *6* (3), 1890-1895.

54. Wang, L.; Zhu, S.-J.; Wang, H.-Y.; Qu, S.-N.; Zhang, Y.-L.; Zhang, J.-H.; Chen, Q.-D.; Xu, H.-L.; Han, W.; Yang, B.; Sun, H.-B., Common Origin of Green Luminescence in Carbon Nanodots and Graphene Quantum Dots. *ACS Nano* **2014,** *8* (3), 2541-2547.

55. Niedziałkowski, P.; Ossowski, T.; Zięba, P.; Cirocka, A.; Rochowski, P.; Pogorzelski, S. J.; Ryl, J.; Sobaszek, M.; Bogdanowicz, R., Poly-l-lysine-modified boron-doped diamond electrodes for the amperometric detection of nucleic acid bases. *Journal of Electroanalytical Chemistry* **2015,** *756*, 84-93.

56. Ding, H.; Yu, S.-B.; Wei, J.-S.; Xiong, H.-M., Full-Color Light-Emitting Carbon Dots with a Surface-State-Controlled Luminescence Mechanism. *ACS Nano* **2016,** *10* (1), 484-491.

57. Ripalda, J. M.; Román, E.; Díaz, N.; Galán, L.; Montero, I.; Comelli, G.; Baraldi, A.; Lizzit, S.; Goldoni, A.; Paolucci, G., Correlation of x-ray absorption and x-ray photoemission spectroscopies in amorphous carbon nitride. *Physical Review B* **1999,** *60* (6), R3705-R3708.

58. Wang, H.; Maiyalagan, T.; Wang, X., Review on Recent Progress in Nitrogen-Doped Graphene: Synthesis, Characterization, and Its Potential Applications. *ACS Catalysis* **2012,** *2* (5), 781-794.

59. Okpalugo, T. I. T.; Papakonstantinou, P.; Murphy, H.; McLaughlin, J.; Brown, N. M. D., High resolution XPS characterization of chemical functionalised MWCNTs and SWCNTs. *Carbon* **2005,** *43* (1), 153-161.

60. Mocci, F.; Olla, C.; Cappai, A.; Corpino, R.; Ricci, P. C.; Chiriu, D.; Salis, M.; Carbonaro, C. M., Formation of Citrazinic Acid Ions and Their Contribution to Optical and Magnetic Features of Carbon Nanodots: A Combined Experimental and Computational Approach. *Materials* **2021,** *14* (4), 770.

61. Stagi, L.; Mura, S.; Malfatti, L.; Carbonaro, C. M.; Ricci, P. C.; Porcu, S.; Secci, F.; Innocenzi, P., Anomalous Optical Properties of Citrazinic Acid under Extreme pH Conditions. *ACS Omega* **2020,** *5* (19), 10958-10964.

62. Maeda, S.; Mori, T.; Sasaki, C.; Kunimoto, K.-K.; Kuwae, A.; Hanai, K., Structural investigation of microbial poly(ε-L-lysine) derivatives with azo dyes by solid-state 13C and 15 N NMR. *Polymer Bulletin*

2005, *53* (4), 259-267.

63. Carrier, D.; Pézolet, M., Raman spectroscopic study of the interaction of poly-L-lysine with dipalmitoylphosphatidylglycerol bilayers. *Biophysical Journal* **1984,** *46* (4), 497-506.

64. Sarkar, S.; Chowdhury, J.; Dutta, S.; Pal, T., A pH dependent Raman and surface enhanced Raman spectroscopic studies of citrazinic acid aided by theoretical calculations. *Spectrochimica Acta Part A: Molecular and Biomolecular Spectroscopy* **2016,** *169*, 108-115.

65. Alemán, B.; Regan, W.; Aloni, S.; Altoe, V.; Alem, N.; Girit, C.; Geng, B.; Maserati, L.; Crommie, M.; Wang, F.; Zettl, A., Transfer-Free Batch Fabrication of Large-Area Suspended Graphene Membranes. *ACS Nano* **2010,** *4* (8), 4762-4768.

66. Ghosh, K.; Kumar, M.; Maruyama, T.; Ando, Y., Tailoring the field emission property of nitrogen-doped carbon nanotubes by controlling the graphitic/pyridinic substitution. *Carbon* **2010,** *48* (1), 191-200.

67. Tang, L.; Ji, R.; Li, X.; Teng, K. S.; Lau, S. P., Energy-level structure of nitrogen-doped graphene quantum dots. *Journal of Materials Chemistry C* **2013,** *1* (32), 4908-4915.

68. Arenal, R.; March, K.; Ewels, C. P.; Rocquefelte, X.; Kociak, M.; Loiseau, A.; Stéphan, O., Atomic Configuration of Nitrogen-Doped Single-Walled Carbon Nanotubes. *Nano Letters* **2014,** *14* (10), 5509-5516.

69. D'Angelo, D.; Bongiorno, C.; Amato, M.; Deretzis, I.; La Magna, A.; Compagnini, G.; Spanò, S. F.; Scalese, S., Electron energy-loss spectra of graphene oxide for the determination of oxygen functionalities. *Carbon* **2015,** *93*, 1034-1041.

70. Mangolini, F.; Li, Z.; Marcus, M. A.; Schneider, R.; Dienwiebel, M., Quantification of the carbon bonding state in amorphous carbon materials: A comparison between EELS and NEXAFS measurements. *Carbon* **2021,** *173*, 557-564.

71. Cappai, A.; Melis, C.; Stagi, L.; Ricci, P. C.; Mocci, F.; Carbonaro, C. M., Insight into the Molecular Model in Carbon Dots through Experimental and Theoretical Analysis of Citrazinic Acid in Aqueous Solution. *The Journal of Physical Chemistry C* **2021,** *125* (8), 4836-4845.

72. Sato, R.; Iso, Y.; Isobe, T., Fluorescence Solvatochromism of Carbon Dot Dispersions Prepared from Phenylenediamine and Optimization of Red Emission. *Langmuir* **2019,** *35* (47), 15257-15266.

73. Yan, D.; Shi, T.; Zang, Z.; Zhou, T.; Liu, Z.; Zhang, Z.; Du, J.; Leng, Y.; Tang, X., Ultrastable CsPbBr3 Perovskite Quantum Dot and Their Enhanced Amplified Spontaneous Emission by Surface Ligand Modification. *Small* **2019,** *15* (23), 1901173.

74. Bai, Y.; Qin, J.; Shi, L.; Zhang, J.; Wang, M.; Zhan, Y.; Zou, H.; Haacke, S.; Hou, X.; Zi, J.; Hu, B., Amplified Spontaneous Emission Realized by Cogrowing Large/Small Grains with Self-Passivating Defects and Aligning Transition Dipoles. *Adv Opt Mater* **2019,** *7* (13), 1900345.

75. Qu, S.; Liu, X.; Guo, X.; Chu, M.; Zhang, L.; Shen, D., Amplified Spontaneous Green Emission and Lasing Emission From Carbon Nanoparticles. *Advanced Functional Materials* **2014,** *24* (18), 2689-2695.

76. Zhang, W. F.; Zhu, H.; Yu, S. F.; Yang, H. Y., Observation of Lasing Emission from Carbon

Nanodots in Organic Solvents. *Advanced Materials* **2012,** *24* (17), 2263-2267.

77. Han, Z.; Ni, Y.; Ren, J.; Zhang, W.; Wang, Y.; Xie, Z.; Zhou, S.; Yu, S. F., Highly efficient and ultra-narrow bandwidth orange emissive carbon dots for microcavity lasers. *Nanoscale* **2019,** *11* (24), 11577-11583.

78. Ni, Y.; Han, Z.; Ren, J.; Wang, Z.; Zhang, W.; Xie, Z.; Shao, Y.; Zhou, S., Ultralow Threshold Lasing from Carbon Dot–Ormosil Gel Hybrid-Based Planar Microcavity. *Nanomaterials* **2021,** *11* (7), 1762.

SYNOPSIS:

The internal structure of polymeric carbon dots (PCDs) on atomically-thin graphene and their applicability as microcavity-integrated optical gain media are reported.